LANGMUIR

pubs.acs.org/Langmuir Article

Molecular Simulation of the Impact of Defects on Electrolyte Intrusion in Zeolites

Ambroise de Izarra, François-Xavier Coudert,* Alain H. Fuchs, and Anne Boutin*

Cite This: *Langmuir* 2023, 39, 19056−19063 Read Online

ACCESS | Metrics & More | Article Recommendations | Supporting Information

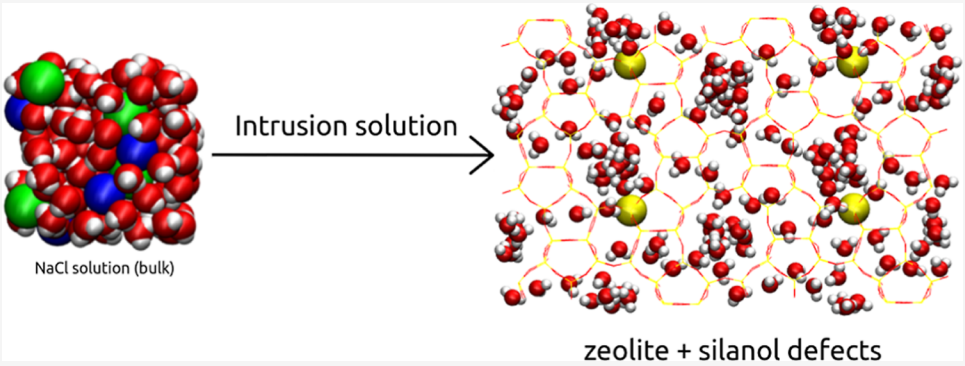

ABSTRACT: We have investigated through molecular simulation the intrusion of electrolytes in two representative pure-silica zeolites, silicalite-1 and chabazite, in which point defects were introduced in varying amounts. We distinguish between two types of defects, considering either "weak" or "strong" silanol nest defects, resulting in different hydration behaviors. In the presence of weak defects, the hydration process occurs through a homogeneous nucleation process, while with strong defects, we observe an initial adsorption followed by a filling of the nanoporous volume at a higher pressure. However, we show that electrolytes do not penetrate the zeolites, and these defects appear to have only marginal influence on the thermodynamics of electrolyte intrusion. While replacing pure water by the electrolyte solution shifts the intrusion pressure toward higher values because of the drop of water saturation vapor pressure, an increase in hydrophilicity of the framework due to point defects has the opposite effect, showing that controlling the amount of defects in zeolites is crucial for storage energy applications.

INTRODUCTION

In the past years, a new field of application in energy storage was discovered for hydrophobic nanoporous materials,[1−8] where the nonwetting liquid penetrates the pores under high pressure, resulting in the conversion of mechanical energy into fluid−solid interface energy. When the pressure is released, the mechanical energy can be restored upon the release of the fluid. Historically, intrusion of water in pure-silica zeolites (also called "zeosils") has been first reported in 2001[9] and represents the starting point of subsequent intrusion and extrusion experiments performed on various zeosils.[10−19] Later, Tzanis and co-workers[20] discovered that replacing pure water by electrolyte solutions is an effective way to increase the mechanical energy stored in zeosils, due to a shift of intrusion pressure toward higher values. For instance, it was shown that the intrusion of a highly concentrated LiCl solution (∼20 M) in silicalite-1 increases the intrusion pressure from 96 MPa (for pure water) to 280 MPa, resulting in an increase of stored energy from 10 to 31 J/g. Since this pioneering work, the influence of the nature of the electrolyte and its concentration on the energetic properties of zeosils has been widely investigated.[21−37]

In a previous study, we have reported a computational investigation of the effect of the electrolyte solution (nature and concentration) on their intrusion pressure in defect-free pure silica zeolites.[38] We found that due to poorer ion solvation in the pores than in the bulk, intrusion of electrolyte solutions starts with only intrusion of pure water (and exclusion of the ions). Moreover, we showed that the shift of intrusion pressure is more complex than a simple osmotic effect because electrolytes are nonideal solutions. Taking into account the water activity, which we calculated by the Pitzer model[39,40] for each electrolyte over a wide range of concentration, can explain the experimental data available.

Pure-silica zeolites consistently display a strong hydrophobic character, but their exact extent can depend on the synthesis

Received: October 31, 2023
Revised: December 1, 2023
Accepted: December 1, 2023
Published: December 13, 2023

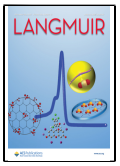

https://doi.org/10.1021/acs.langmuir.3c03306
Langmuir 2023, 39, 19056−19063

conditions of the material. Zeosils are typically obtained through hydrothermal synthesis[41] using fluoride (F^-) or hydroxide (HO^-) anions. Patarin and co-workers[9] highlighted that the intrusion pressure of water was higher for silicalite-1 (F^-) than for silicalite-1 (OH^-), differing by 20 MPa. This shift of intrusion pressure may be attributed to the presence of internal defects in the framework, as silicalite-1 synthesized through the hydroxide route is known to contain more defects than using the fluoride route.[42−44] Recently, it has been shown that the intrusion of NaCl electrolyte solution in chabazite occurs in two steps:[21] first, only water molecules penetrate into the nanocages at 44 MPa, followed by the intrusion of the ions at ∼260 MPa. The Rietveld analysis of the high-pressure phase revealed that the Na^+ cation interacts with the oxygen atom of the framework, while the Cl^- anion is very close to the silanol defects. This motivated the present work where we investigate several models of silicalite-1 and chabazite containing point defects in order to probe their influence on electrolyte intrusion in the zeosils.

In the same manner as in the previous works of Cailliez and Trzpit,[11,45] we tune the hydrophobicity of the framework by introducing various amounts of hydrophilic defects, modeled as silanol nests, to qualitatively reproduce the change in adsorption thermodynamics in zeolites as a function of the number and strength of defects. These defects cause the zeolites to become less hydrophobic and more hydrophilic because the water−zeolite interaction energy increases and becomes higher than the bulk cohesion energy of water (which is of −44 kJ mol^{-1} in the TIP4P model). Starting from equilibrated zeolite−water systems, we attempt to introduce electrolyte pairs (or triplets in case of divalent-cation electrolytes) inside the frameworks. Our simulations highlight that silanol defects have very little influence on electrolyte solvation compared to defect-free zeolite frameworks: the thermodynamic work performed to introduce a first electrolyte unit in the system is similar to that in defect-free frameworks. We conclude that point defects, such as silanol nests, do not provide a satisfactory explanation per se for the electrolyte intrusion in zeolites observed in some experimental cases.

MATERIALS AND METHODS

Zeolite Models. We used rigid zeolite frameworks and the atomic coordinates of the orthorhombic (*Pnma*) structure of silicalite-1 determined by Olson et al.[46] (unit cell parameters: a = 20.07 Å; b = 19.92 Å; c = 13.42 Å) and the trigonal ($R\bar{3}m$) structure of chabazite determined by Calligaris et al.[47] (unit cell parameters: $a = b = c$ = 9.459 Å; $\alpha = \beta = \gamma$ = 94.07°). The simulation boxes contain, respectively, four and 12 unit cells for silicalite-1 and chabazite, in order to have large enough systems to avoid side effects due to use of periodic boundary conditions. Due to the strong nature of the Si−O bonds, changes in zeolite structure upon water and electrolyte adsorption are generally small[21] and the rigid framework approach is a realistic approximation.[48]

Defect Model. It is known from NMR experiments that silanol defects are among the most common points defects encountered in zeolites.[49] These defects are modeled through a silicon atom vacancy, resulting in a "silanol nest" initially proposed by Barrer[50] and integrated in silicalite-1 by Cailliez and Trzpit[11,45] to study its influence on water intrusion. We have chosen here to introduce 1 or 4 silanol nests in each unit cell of the silicalite-1 model and 0.25 or 0.5 nests in each unit cell of the chabazite model (see Figure 1). We decided to focus our attention on these two zeolites to disentangle the role of silanol defects on the thermodynamic of electrolyte intrusion, from that of pore size. In the silicalite-1 model, we selected and removed from the framework a silicon atom at the intersection between a straight and a zigzag channel (T1 site). For chabazite, we chose to remove a silicon atom that was common to both large and small cages. The resulting four dangling oxygen atoms were then saturated by a hydrogen atom and the O−H bond length (0.9572 Å) was set to the same value as in the TI4P water molecule model, as well as the Si−O−H angle set to 109.5°. In real zeolites, the silanol defects are most often assumed to be randomly distributed—although some recent studies have shown the potential for multiple connected defects to exist in specific cases.[51] We discard here frameworks having irregular defect distribution because the use of periodic boundary conditions would lead to spurious effect, but instead use a regular spacing of the defects.[11,45] It must be mentioned here that we are not exploring high defect content models because it has been proven that the silicalite-1 model containing only one defect per cell provides a reasonable description of the thermodynamics of water intrusion.[11]

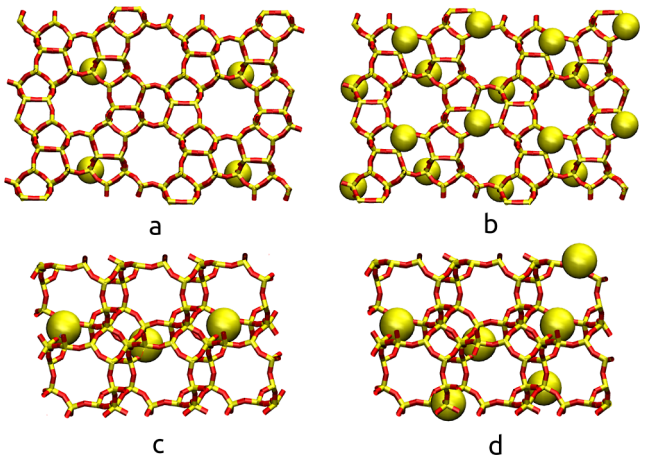

Figure 1. Schematic view of four unit cells of the silicalite-1 structure and 12 unit cells of the chabazite structure along the b axis with defects show as yellow spheres. (a) Model of silicalite-1 with 1 silanol nest defect per unit cell. (b) Model of silicalite-1 with 4 defects per unit cell. (c) Model of chabazite with 0.25 silanol nest defect per unit cell. (d) Model of chabazite with 0.5 silanol nest defect per unit cell.

Local Defect Optimization Procedure. After the introduction of silanol defects as described above, we performed a local optimization of the defect structure using the force field described in the next section by allowing each H atom to freely rotate around the Si−O bond, while the rest of the framework remains frozen. We used the RASPA simulation package[52] in which we implemented the version of the pivot algorithm proposed by Steinhauser.[53] For each oxygen atom in a triplet Si−O−H, we define the unit vector $\vec{n}$ pointing from Si to the O atom

$$\vec{n} = \frac{\overrightarrow{\mathrm{SiO}}}{\left\|\overrightarrow{\mathrm{SiO}}\right\|} \tag{1}$$

Then, the vector $\overrightarrow{\mathrm{OH}}$ is rotated of an angle α around the direction **n** and the new coordinate of the H atom $\overrightarrow{\mathrm{OH}'}$ is calculated using the following relationship

$$\overrightarrow{\mathrm{OH}'} = \overrightarrow{\mathrm{OH}}\cos\alpha + (1-\cos\alpha)(\overrightarrow{\mathrm{OH}}\cdot\vec{n})\vec{n} + \sin\alpha(\vec{n}\times\overrightarrow{\mathrm{OH}}) \tag{2}$$

The new hydrogen atom coordinates are accepted according to the Metropolis criterion. For each structure, we run 200,000 MC pivot moves for which a hydrogen H of the framework is chosen randomly. An example of some of resulting silanol nests after optimization in silicalite-1 and chabazite are presented in Figure 2.

We notice that three silanol groups are involved in a trimer of hydrogen bonds characterized by an imperfect O−H−O alignment, resulting from the applied steric constraints. These silanol nest geometric structures are in very good agreement with classical studies

https://doi.org/10.1021/acs.langmuir.3c03306
Langmuir 2023, 39, 19056−19063

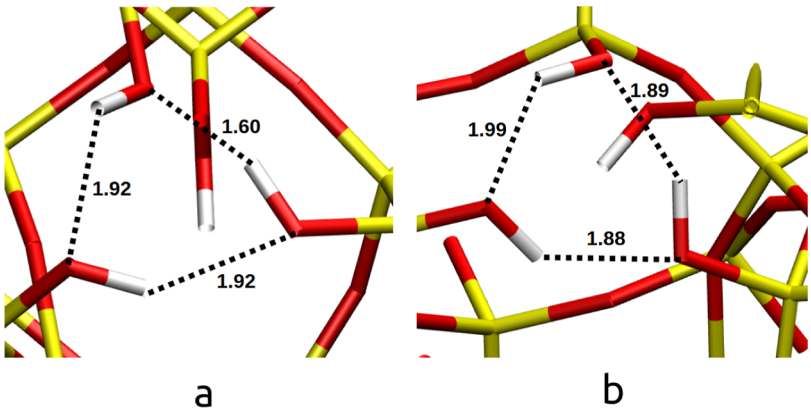

Figure 2. Silanol nest defects obtained from the local optimization procedure in silicalite-1 (a) and chabazite (b). The H atoms are colored gray, and the hydrogen bond lengths are labeled in Å.

of Trzpit and Cailliez,[11,45] the DFT calculations of Sokol et al.,[54] as well as those obtained from ab initio cluster calculations.[55]

Force Field. Molecular simulations were performed in the classical limit, with no bond breaking or formation, meaning that the materials undergo no structural change upon the intrusion of water or electrolyte. We used the force field proposed by Desbiens and co-workers,[56] tailored to reproduce intrusion of TIP4P water around ∼100 MPa in defect-free silicalite-1, within the rigid framework approach and the Kiselev approximations.[48] Hence, the partial charges of both framework oxygen and silicon atoms were fixed to −0.6*e* and +1.2*e* respectively (see Table S1). Regarding the silanol nest defect, we distribute the charge carried by the vacant silicon atom on the four hydrogen atoms in order to keep the zeolite neutral. We distinguish between two types of defects that differ only by their charge distribution:[11] the so-called "weak defect" results from a partial charge of +0.3*e* carried by each hydrogen atom, while the "strong" defect has the partial charge of hydrogen atom increased to +0.6*e* and its oxygen charge decreased accordingly (Table S2). Water molecules are modeled with the rigid TIP4P model[57] and the electrolytes are represented as point charges and Lennard-Jones centers. We considered the following monovalent electrolytes: LiCl, NaCl, KCl, RbCl, CsCl, KF, KBr, and KI. We also explored the following divalent electrolytes to probe the influence of charge ion: $MgCl_2$, $CaCl_2$, $SrCl_2$, and $BaCl_2$. The details of the force field are given in Tables S3, S4, and S5.[58,59]

We used Lorentz−Berthelot mixing rules for cross-terms in the Lennard-Jones potential, and Ewald summation was used to account efficiently for electrostatic interactions. We used a cutoff of 8.0 Å for both the Lennard-Jones potential and the separation between the real space and reciprocal space in the Ewald summation.

Adsorption of Water and Electrolytes. Adsorption isotherms of pure water in the zeolites were computed with GCMC simulations using the RASPA simulation package.[52] We screened several values of the chemical potential of the (fictitious) bulk fluid reservoir to compute the number of adsorbed water molecules, by using the relationship between chemical potential of water and hydrostatic pressure $\mu_{water}(P)$.[56] In order to explore the phase space, translation, rotation, and swap moves were applied to water molecules, in a ratio of 1:1:2, respectively. Each simulation consists of 4×10^5 equilibration cycles followed by 2×10^5 production cycles where the average quantities were calculated. In addition, we characterized the thermodynamics of water intrusion by showing the evolution of the potential energy per water molecule as a function of intrusion pressure.

In order to probe electrolyte insertion in zeolites, we used our recent implementation of the nonequilibrium candidate Monte Carlo (NCMC) move[60] in the osmotic ensemble with a relative probability set to 10^{-3}. The starting configurations were the silicalite-1 and chabazite materials in equilibrium with a water reservoir at 400 and 200 MPa, respectively, in which we will attempt to introduce ion pairs. Briefly, the osmotic ensemble is sampled using a hybrid Monte Carlo move using nonequilibrium molecular dynamics, or NCMC, initially proposed by Nilmeier[61] and later applied by Ross and co-workers[62] to sample the distribution of NaCl electrolyte around biomolecules. We previously calculated the chemical potential of ion exchange $\Delta\mu_{C_nA_m}(P)$ in the semigrand canonical ensemble for "alchemically" transforming $(n + m)$ water molecules chosen randomly into an electrolyte unit C_nA_m (where C^{m+} and A^{n-} are the ionic species) in bulk electrolyte solution at fixed concentration. This chemical potential, used in combination with NCMC moves to insert or delete ions at a constant number of particles in the system, defines the osmotic ensemble, where the fictitious reservoir is an electrolyte solution at a concentration imposed by the chemical potential. We tabulated this quantity in our previous work and use here the values corresponding to molalities of 4.77 and 4.62 mol/kg for monovalent and divalent bulk electrolytes, respectively.[38] The NCMC move consists of $\mathcal{T}$=200 steps, each one involving a perturbation of the system through interpolation of nonbonded parameters of the chosen molecules to be transformed, followed by 200 MD relaxation steps with a time step of 1 fs in the *NVE* ensemble. All simulations used a Nosé−Hoover thermostat, setting the temperature at 300 K. In addition, translations were performed on both ions and water, while rotations were applied only to water molecules, in a ratio of 1:1:1. Simulation is performed until 1000 moves in the osmotic ensemble have been attempted.

RESULTS AND DISCUSSION

Influence of Defects on Water Intrusion. We first investigated the effect of local defects on pure water intrusion inside silicalite-1 and chabazite. In Figure 3, we plot the intrusion isotherm of TIP4P water using GCMC simulations for the defect-free model of silicalite-1 and chabazite and compare it to the isotherms with either weak or strong silanol defects. The "weak" silanol defect model provides a representation of defects observed in zeolites synthesized in hydroxide (HO^-) media. In order to keep a zeolite model as simple as possible, the "strong" defect model attempts to mimic more hydrophilic defects, such as $Si-O^-$, Na^+ without modifying the defect geometry, but only its charge distribution.[11,45]

Let us first discuss the intrusion of water in the presence of weak defects. In all cases, the isotherms are of type V according to the IUPAC classification,[63] and condensation takes place above bulk water vapor pressure ($P_0 \sim 5300$ Pa for the TIP4P model[56]), as in the case of the defect-free models. This indicates that the framework system remains hydrophobic, regardless of the defect content.[11] By increasing the number of

https://doi.org/10.1021/acs.langmuir.3c03306
Langmuir 2023, 39, 19056−19063

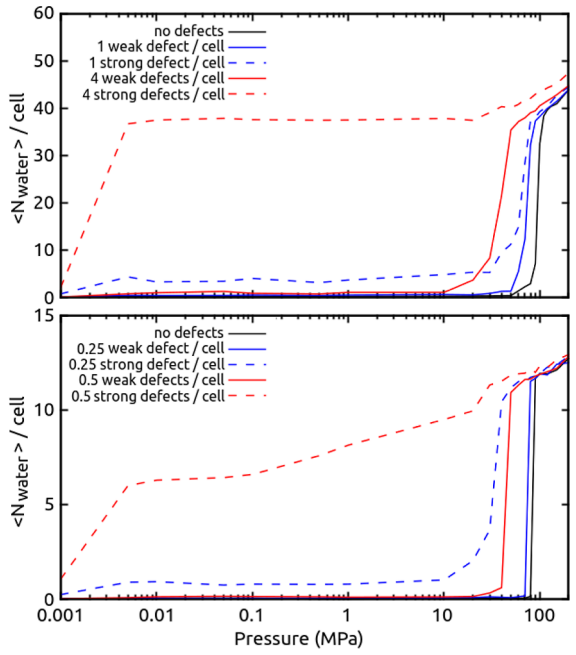

Figure 3. Water intrusion isotherms computed through GCMC simulations at 300 K for silicalite-1 (top) and chabazite (bottom). Black curves correspond to defect-free zeolites. Blue and red full curves: models with weak silanol nest defects. Blue and red dashed curves: models with strong silanol nest defects.

defects, the forced intrusion (capillary evaporation) is shifted toward lower pressure. The similarity of the qualitative hydration behavior regardless of defect content (i.e., the same shape of the isotherms) is worth being examined in more detail by probing the thermodynamics of water intrusion. In Figure 4, we show the evolution of potential energy per water molecule adsorbed in silicalite-1 and chabazite as a function of water pressure.

In the presence of weak defects (top and bottom left panels on Figure 4), the evolution of potential energy is consistent with the hydrophobic nature of the framework because, at low water content, the potential energy per water molecule is below the bulk cohesion energy of water—indicating that water would rather stay in the bulk rather than penetrate the framework. The presence of defects helps lowering the water−water energy to −27 kJ mol^{-1} $molec^{-1}$ for silicalite-1 and −32 kJ mol^{-1} $molec^{-1}$ for chabazite upon condensation, occurring at lower intrusion pressure in the presence of weak defects (e.g., around ∼70 and 40 MPa in silicalite-1 for 1 and 4 defects per cell, and ∼80 and 50 MPa in chabazite for 0.25 and 0.50 defects per cell) than for defect-free zeolites (e.g., 95 MPa for silicalite-1 and 90 MPa for chabazite). Hence, the water−water interaction energy is dominant in the condensation mechanism and results in a total energy of −40 kJ mol^{-1} $molec^{-1}$ which is close to the bulk liquid value. The snapshots of water intrusion in silicalite-1 containing one weak defect per cell (see Figure S1) confirm that the condensation of water occurs through a rather homogeneous nucleation of water molecules, followed by a collapse of the water cluster into the bulk phase, as for defect-free silicalite-1.[45]

In the presence of strong defects, however, the picture is drastically changed and the isotherms progressively transition from type V to type IV (Figure 3). This evolution observed for silicalite-1 is in agreement with previous studies:[11,45] there is

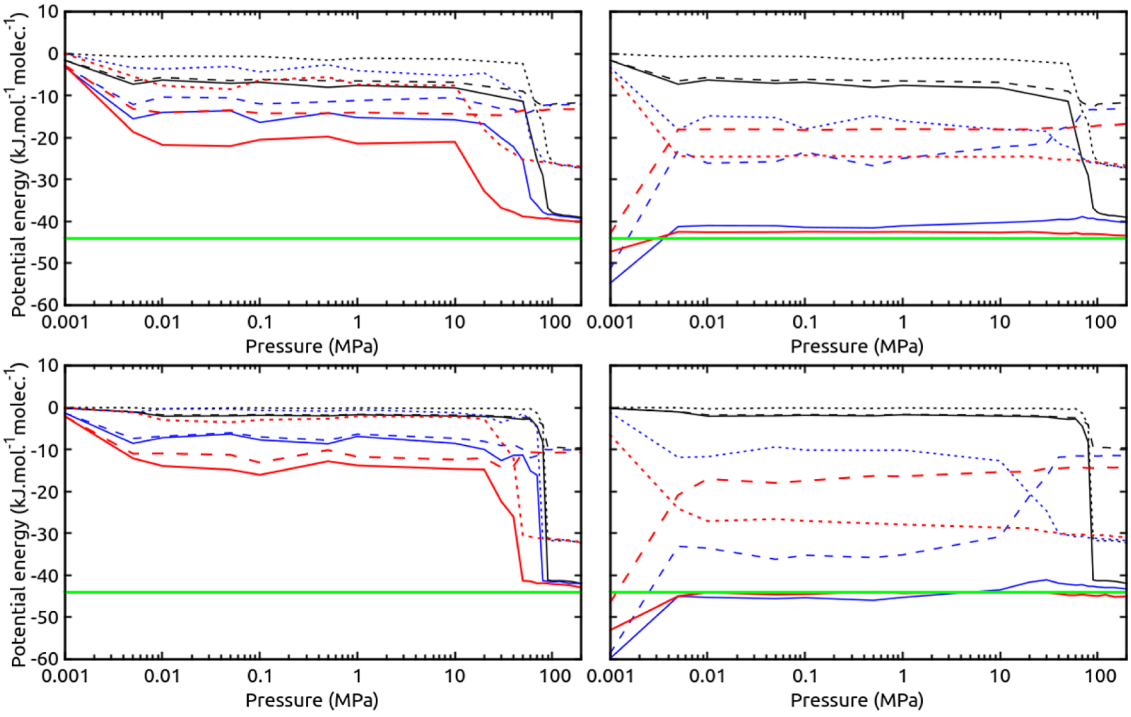

Figure 4. Potential energy per water molecule as a function of water pressure for various models of silicalite-1 (top panels) and chabazite (bottom panels). Left: weak defects; right: strong defects. The total potential energy (represented in solid lines) is split into two contributions: the water−zeolite energy (dashed lines) and the water−water energy (dotted lines). Black curves: defect-free zeolites; blue curves: low defect concentration (1 defect per cell in silicalite-1; 0.25 defect per cell in chabazite); and red curves: large defect concentration (4 defects per cell in silicalite-1; 0.50 defect per cell in chabazite). The green horizontal line indicates bulk cohesion energy of water at 300 K.

https://doi.org/10.1021/acs.langmuir.3c03306
Langmuir 2023, 39, 19056−19063

some water uptake at low pressure and the transition is less sharp when the defect content is increased. When strong defects are present, the water−zeolite interaction becomes the dominant factor in the condensation process, as it becomes larger than the bulk cohesion energy of water at very low pressure. In that case, nucleation of water happens more heterogeneously at low pressure, around the defect sites, and each of these small water clusters acts as a seed in the condensation at higher pressure. This is shown by MC snapshots illustrating the heterogeneous nature of water condensation for silicalite-1 around the strong defects (Figure 5). The type IV nature of the observed isotherms is thus

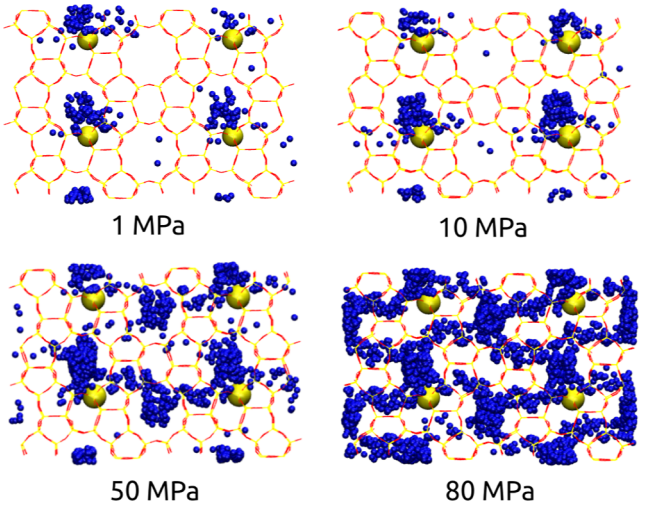

Figure 5. Framework of silicalite-1 with 1 strong defect per unit cell and density of adsorbed water as a cloud of blue spheres for various values of intrusion pressure.

explained by the favorable adsorption of a moderate amount of water around the strong defects, followed by a sudden filling of the nanoporous volume. The effect of various type of silanol defects on water intrusion in silicalite-1 and chabazite are in qualitative agreement with previous studies focused on silicalite-1.[11,45]

Influence of Defects on Electrolyte Intrusion. We now turn our attention to the impact of these weak and strong defects on the adsorption of electrolytes inside the nanopores of the zeolites. Despite the large body of literature on the intrusion of electrolyte solutions in zeolites, there have been very few studies attempting to characterize the composition of the intruded fluid, especially as a function of the intrusion pressure.[21,22,30] The behavior most commonly observed is that water molecules penetrate the nanoporous volume at intrusion pressure, potentially followed by electrolyte penetration at a much higher pressure (e.g., around 1 order of magnitude of increase in case of 2 mol/L NaCl solution in chabazite[21]). Because previous molecular simulations of electrolyte intrusion in defect-free zeolites showed that ions intrusion is thermodynamically unfavorable in the sub-GPa range of pressure,[60] our goal was to probe electrolyte intrusion in those same zeolites in the presence of point defects.

Therefore, we performed MC simulations in the osmotic ensemble in order to insert a first electrolyte unit in water, with zeolite systems originally equilibrated with a water reservoir at values of pressure that represent saturation uptake: 400 MPa for silicalite-1 and 200 MPa for chabazite. From these starting configurations, Figure 6 reports the histograms of the alchemical work associated with the insertion of a single NaCl pair in various zeolite model containing defects. In this analysis, we discarded both the silicalite-1 and chabazite models containing, respectively, 4 and 0.5 strong silanol defects per unit cell because of their hydrophilic character which does not mimic the experimental behavior. For all other zeolite models, we can see that the profile of the alchemical work histogram is similar in both shape, average, and extent to the parent defect-free zeolite. This shows that the presence of defects, although it strongly impacts the adsorption of water, has a marginal influence on the thermodynamics of electrolyte intrusion.

In order to provide an estimation of the acceptance probability of the insertion of an NaCl pair, we plot a vertical line in each histogram of Figure 6, indicating the value of the alchemical work associated with an intrusion probability of 10^{-2} for a NaCl electrolyte at molality of 4.77 mol/kg using the following acceptance probability[38]

$$P_{\mathrm{acc}} = \min\left(1, \frac{\prod_{i=0}^{m+n-1}(N_{\mathrm{H_2O}} - i)}{\prod_{j=1}^{n}(N_{C^{m+}} + j)\prod_{k=1}^{m}(N_{A^{n-}} + k)} e^{-\beta(W_{C_nA_m} - \Delta\mu_{C_nA_m})}\right)$$
$$= \min\left(1, N_{\mathrm{H_2O}}(N_{\mathrm{H_2O}} - 1)e^{-\beta(W_{C_nA_m} - \Delta\mu_{C_nA_m})}\right) \quad (3)$$

All MC moves attempted to insert a NaCl unit in the zeolites filled with water were rejected, and registered values of W used to construct the histograms are associated with much lower insertion probabilities. This enables us to conclude that in the frame of our model, electrolyte does not penetrate inside the zeolites. On the microscopic scale, a silanol defect is not singularly different from a water molecule because the silanol hydroxyl group plays the same role in solvating the Cl^- anion as those of the water molecule. The intrusion and extrusion of various electrolyte (NaCl, NaBr, and $CaCl_2$) at 2 and 3 M in pure-silica chabazite has been investigated in detail in an earlier work to be discussed in the context of our simulations.[21] Characterizations of chabazite samples before and after intrusion using ^{29}Si solid-state NMR spectroscopy confirm formation of silanol defects upon intrusion of NaCl electrolyte solution, resulting in a lowering of the intrusion pressure in the second and third intrusion cycle, from 54 to 47 and 44 to 38 MPa for, respectively, 2 and 3 M solutions. This indicates that despite increasing the amount of silanol defects in the chabazite, it remains hydrophobic.

A detailed investigation of the nature of the intruded fluid obtained by Rietveld analysis shows that water molecules penetrate first chabazite at the intrusion pressures of 54 and 60 MPa for 2 M NaCl and $CaCl_2$, respectively, followed by electrolyte intrusion at a much higher pressure of ∼250 and ∼600 MPa and the concentration inside the chabazite is found to be much higher than those of the bulk, closed to the saturation concentration. Once intruded, it is shown that electrolyte interferes with silanol defects, but it does not mean in absolute that silanol defects would result in itself on electrolyte intrusion at a higher concentration than the bulk. The nonintrusion of electrolyte is consistent with experiments reporting only penetration of water molecules at the intrusion pressure, but the reported intrusion of electrolyte at a much

https://doi.org/10.1021/acs.langmuir.3c03306
Langmuir 2023, 39, 19056−19063

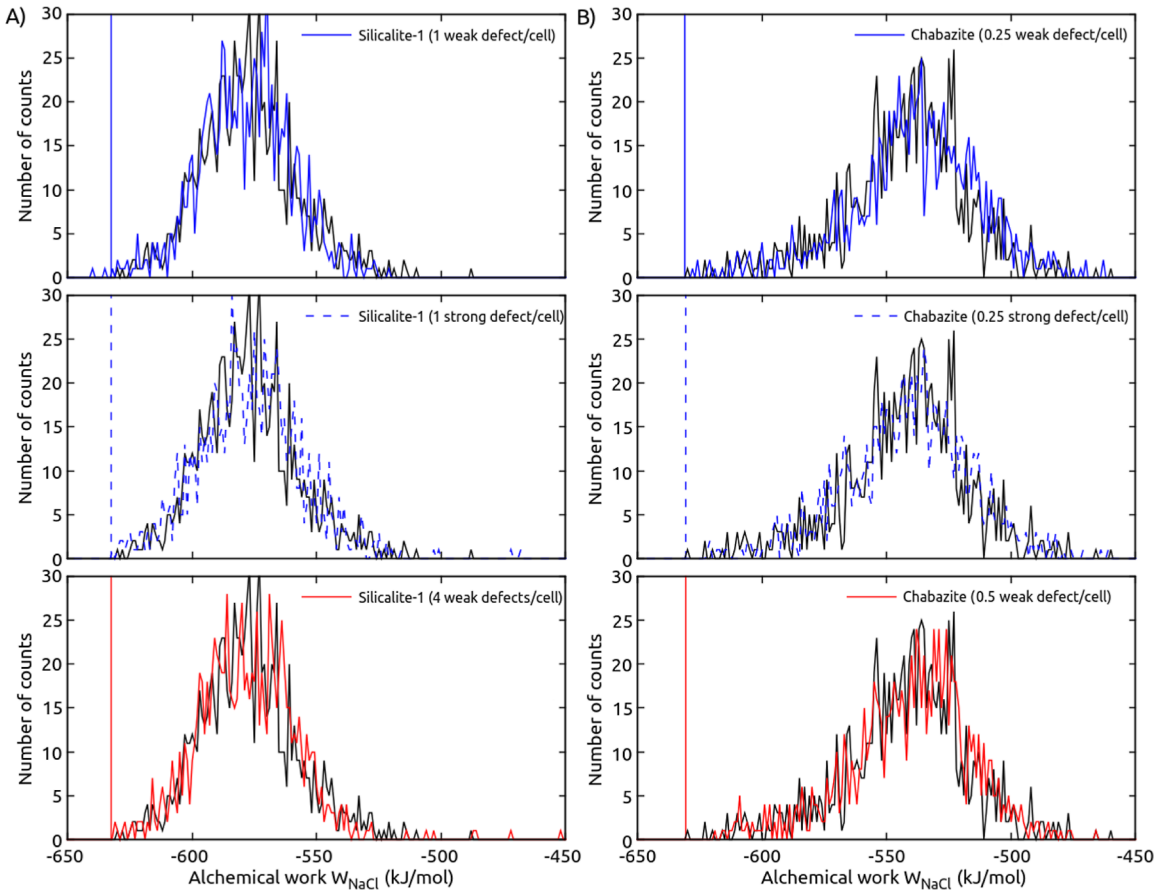

Figure 6. Histogram of the alchemical work for inserting a NaCl electrolyte unit W_{NaCl} in various defect models of silicalite-1 (left panel A) and chabazite (right panel, B). The vertical lines indicate the value of W_{NaCl} corresponding to an insertion probability of $P_{acc} = 10^{-2}$ for a NaCl electrolyte solution at molality of 4.77 mol/kg. For comparison, the histogram of alchemical work for defect-free zeolites is displayed in black for each case.

higher pressure may not be accessible due to limits of both force field and classical simulations. First, the force field used to model interactions within the zeolites is tailored to reproduce the intrusion of TIP4P water in silicalite-1 and may not be relevant to describe properly interaction with water at very high pressure. Second, the use of our current empirical force field to model electrolyte by a simple electrostatic potential coupled with the Lennard-Jones interaction does not take into account polarizability, charge transfer or use of unreduced Coulomb interactions, that may be relevant at higher pressures.[64]

CONCLUSIONS

In this work, we have investigated in detail how the hydration thermodynamics and electrolyte intrusion in silicalite-1 and chabazite zeolites are affected by introducing various amounts of attractive point defects (modeled by silanol nests) into the parent pure-silica zeolites. First, we reproduced qualitatively the evolution of hydration as a function of the strength of silanol defects introduced in the zeolites. In the presence of "weak" defects, the adsorption isotherms for both chabazite and silicalite-1 are of type V (according to IUPAC classification). The effect of weak defects is to make the framework more attractive, as shown by a slight shift of the condensation transition, although the frameworks remain hydrophobic. As for defect-free zeolites, the condensation transition occurs through a homogeneous nucleation process. In the case of "strong" defects, the isotherms shift to type IV. The first stage of water loading is attributed to a heterogeneous nucleation of water around the defects, forming small water clusters. The next stage consists of the growth of these clusters of water acting as a seed to trigger the condensation transition.

Then, we probed the influence of defects on electrolyte intrusion. Our simulations in the osmotic ensemble reveal that the alchemical work associated with electrolyte intrusion is similar to that computed in defect-free zeolites and that the probability of electrolyte intrusion is very low. Consequently, silanol defects may not explain electrolyte intrusion in the approximation of our force field and classical simulations. The nonpenetration of electrolyte observed in our simulations is consistent with experimental reporting, with water as the only species intruded in the chabazite at the intrusion pressure. The intrusion of electrolyte occurs at several orders of magnitude higher than the intrusion pressure, and our simulations may not grasp this phenomenon: our force field describing the "rigid host" framework within the Kiselev approximation is specifically tailored to reproduce the intrusion of TIP4P water in silicalite-1 and electrolyte ions are simply described by charged beads ignored polarizability or charge transfer. The present study shows, in any case, that the attractive nature of the defects does not compensate for the thermodynamic cost of desolvation of the ions from the bulk electrolyte. While this could be possible with defects of a stronger nature, they would then turn the zeolite hydrophilic overall.

https://doi.org/10.1021/acs.langmuir.3c03306
Langmuir 2023, 39, 19056−19063

■ ASSOCIATED CONTENT

Supporting Information

The Supporting Information is available free of charge at https://pubs.acs.org/doi/10.1021/acs.langmuir.3c03306.

Force field parameters, Monte Carlo snapshots of silicalite-1 containing 1 weak defect per cell, and raw data of alchemical work extracted from MC simulations in the osmotic ensemble (PDF)

■ AUTHOR INFORMATION

Corresponding Authors

François-Xavier Coudert − *Chimie ParisTech, PSL University, CNRS, Institut de Recherche de Chimie Paris, 75005 Paris, France;* orcid.org/0000-0001-5318-3910; Email: fx.coudert@chimieparistech.psl.eu

Anne Boutin − *PASTEUR, Département de Chimie, École Normale Supérieure, PSL University, Sorbonne Université, CNRS, 75005 Paris, France;* orcid.org/0000-0003-4209-1652; Email: anne.boutin@ens.psl.eu

Authors

Ambroise de Izarra − *PASTEUR, Département de Chimie, École Normale Supérieure, PSL University, Sorbonne Université, CNRS, 75005 Paris, France; Chimie ParisTech, PSL University, CNRS, Institut de Recherche de Chimie Paris, 75005 Paris, France*

Alain H. Fuchs − *Chimie ParisTech, PSL University, CNRS, Institut de Recherche de Chimie Paris, 75005 Paris, France*

Complete contact information is available at: https://pubs.acs.org/10.1021/acs.langmuir.3c03306

Notes

The authors declare no competing financial interest.

■ ACKNOWLEDGMENTS

This work was funded by Agence Nationale de la Recherche under project MESAMM (ANR-19-CE05-0031). Access to high-performance computing platforms was provided by GENCI grant A0150807069.

■ REFERENCES

(1) Eroshenko, V. Heterogeneous energy accumulation or dissipation structure, methods for using such structure and associated apparatus. WO 1996018040 A1, 1996.

(2) Eroshenko, V. Eroshenko hydrocapillary accumulator. WO 1996018040 A1, 1985.

(3) Popyk, A.; Eroshenko, V. Current Status and Perspectives of the Thermomolecular Engine Developing. *Int. J. Thermodyn.* **2014**, *17*, 33.

(4) Coiffard, L.; Eroshenko, V. A.; Grolier, J.-P. E. Thermomechanics of the variation of interfaces in heterogeneous lyophobic systems. *AIChE J.* **2005**, *51*, 1246−1257.

(5) Laouir, A.; Luo, L.; Tondeur, D.; Cachot, T.; Le Goff, P. Thermal machines based on surface energy of wetting: Thermodynamic analysis. *AIChE J.* **2003**, *49*, 764−781.

(6) Eroshenko, V.; Piatiletov, I.; Coiffard, L.; Stoudenets, V. A new paradigm of mechanical energy dissipation. Part 2: Experimental investigation and effectiveness of a novel car damper. *Proc. Inst. Mech. Eng., Part D* **2007**, *221*, 301−312.

(7) Eroshenko, V. A new paradigm of mechanical energy dissipation. Part 1: theoretical aspects and practical solutions. *Proc. Inst. Mech. Eng., Part D* **2007**, *221*, 285−300.

(8) Suciu, C. V.; Iwatsubo, T.; Yaguchi, K.; Ikenaga, M. Novel and global approach of the complex and interconnected phenomena related to the contact line movement past a solid surface from hydrophobized silica gel. *J. Colloid Interface Sci.* **2005**, *283*, 196−214.

(9) Eroshenko, V.; Regis, R.-C.; Soulard, M.; Patarin, J. Energetics: a new field of applications for hydrophobic zeolites. *J. Am. Chem. Soc.* **2001**, *123*, 8129−8130.

(10) Trzpit, M.; Soulard, M.; Patarin, J. The pure silica Chabazite: A high volume molecular spring at low pressure for energy storage. *Chem. Lett.* **2007**, *36*, 980−981.

(11) Trzpit, M.; Soulard, M.; Patarin, J.; Desbiens, N.; Cailliez, F.; Boutin, A.; Demachy, I.; Fuchs, A. The effect of local defects on water adsorption in silicalite-1 zeolite: A joint experimental and molecular simulation study. *Langmuir* **2007**, *23*, 10131−10139.

(12) Cailliez, F.; Trzpit, M.; Soulard, M.; Demachy, I.; Boutin, A.; Patarin, J.; Fuchs, A. H. Thermodynamics of water intrusion in nanoporous hydrophobic solids. *Phys. Chem. Chem. Phys.* **2008**, *10*, 4817−4826.

(13) Trzpit, M.; Rigolet, S.; Paillaud, J.-L.; Marichal, C.; Soulard, M.; Patarin, J. Pure Silica Chabazite Molecular Spring: A Structural Study on Water Intrusion- Extrusion Processes. *J. Phys. Chem. B* **2008**, *112*, 7257−7266.

(14) Saada, M. A.; Rigolet, S.; Paillaud, J.-L.; Bats, N.; Soulard, M.; Patarin, J. Investigation of the energetic performance of pure silica ITQ-4 (IFR) zeolite under high pressure water intrusion. *J. Phys. Chem. C* **2010**, *114*, 11650−11658.

(15) Saada, M. A.; Soulard, M.; Marler, B.; Gies, H.; Patarin, J. High-pressure water intrusion investigation of pure silica RUB-41 and S-SOD zeolite materials. *J. Phys. Chem. C* **2011**, *115*, 425−430.

(16) Tzanis, L.; Trzpit, M.; Soulard, M.; Patarin, J. High pressure water intrusion investigation of pure silica 1D channel AFI, MTW and TON-type zeolites. *Microporous Mesoporous Mater.* **2011**, *146*, 119−126.

(17) Tzanis, L.; Trzpit, M.; Soulard, M.; Patarin, J. Energetic performances of channel and cage-type zeosils. *J. Phys. Chem. C* **2012**, *116*, 20389−20395.

(18) Tzanis, L.; Marler, B.; Gies, H.; Patarin, J. High-pressure water intrusion investigation of pure silica ITQ-7 zeolite. *J. Phys. Chem. C* **2013**, *117*, 4098−4103.

(19) Khay, I.; Tzanis, L.; Daou, T. J.; Nouali, H.; Ryzhikov, A.; Patarin, J. Energetic behavior of the pure silica ITQ-12 (ITW) zeolite under high pressure water intrusion. *Phys. Chem. Chem. Phys.* **2013**, *15*, 20320−20325.

(20) Tzanis, L.; Nouali, H.; Daou, T. J.; Soulard, M.; Patarin, J. Influence of the aqueous medium on the energetic performances of silicalite-1. *Mater. Lett.* **2014**, *115*, 229−232.

(21) Confalonieri, G.; Ryzhikov, A.; Arletti, R.; Nouali, H.; Quartieri, S.; Daou, T. J.; Patarin, J. Intrusion−extrusion of electrolyte aqueous solutions in pure silica chabazite by in situ high pressure synchrotron X-ray powder diffraction. *J. Phys. Chem. C* **2018**, *122*, 28001−28012.

(22) Arletti, R.; Ronchi, L.; Quartieri, S.; Vezzalini, G.; Ryzhikov, A.; Nouali, H.; Daou, T. J.; Patarin, J. Intrusion-extrusion experiments of $MgCl_2$ aqueous solution in pure silica ferrierite: Evidence of the nature of intruded liquid by in situ high pressure synchrotron X-ray powder diffraction. *Microporous Mesoporous Mater.* **2016**, *235*, 253−260.

(23) Ryzhikov, A.; Nouali, H.; Daou, T.; Patarin, J. A drastic influence of the anion nature and concentration on high pressure intrusion−extrusion of electrolyte solutions in Silicalite-1. *Phys. Chem. Chem. Phys.* **2018**, *20*, 6462−6468.

(24) Khay, I.; Daou, T.; Nouali, H.; Ryzhikov, A.; Rigolet, S.; Patarin, J. High pressure intrusion−extrusion of LiCl aqueous solutions in silicalite-1 zeolite: influence on energetic performances. *J. Phys. Chem. C* **2014**, *118*, 3935−3941.

(25) Ryzhikov, A.; Khay, I.; Nouali, H.; Daou, T.; Patarin, J. Drastic change of the intrusion−extrusion behavior of electrolyte solutions in pure silica *BEA-type zeolite. *Phys. Chem. Chem. Phys.* **2014**, *16*, 17893−17899.

(26) Kirschhock, C. E.; De Prins, M.; Verheijen, E.; Ryzhikov, A.; Jean Daou, T.; Nouali, H.; Taulelle, F.; Martens, J. A.; Patarin, J.

Intrusion−extrusion spring performance of−COK-14 zeolite enhanced by structural changes. *Phys. Chem. Chem. Phys.* **2016**, *18*, 18795−18801.
(27) Ronchi, L.; Ryzhikov, A.; Nouali, H.; Daou, T. J.; Patarin, J. Energetic performances of FER-type zeolite in the presence of electrolyte solutions under high pressure. *Energy* **2017**, *130*, 29−37.
(28) Kabalan, I.; Khay, I.; Nouali, H.; Ryzhikov, A.; Lebeau, B.; Albrecht, S.; Rigolet, S.; Fadlallah, M.-B.; Toufaily, J.; Hamieh, T.; et al. Influence of the particle sizes on the energetic performances of MFI-type zeolites. *J. Phys. Chem. C* **2015**, *119*, 18074−18083.
(29) Ronchi, L.; Ryzhikov, A.; Nouali, H.; Daou, T. J.; Patarin, J. Energetic performances of pure-silica DDR zeolite by high-pressure intrusion−extrusion of electrolyte aqueous solutions: A shock-absorber with huge absorbed energy. *J. Phys. Chem. C* **2018**, *122*, 2726−2733.
(30) Confalonieri, G.; Ryzhikov, A.; Arletti, R.; Quartieri, S.; Vezzalini, G.; Isaac, C.; Paillaud, J.-L.; Nouali, H.; Daou, T. J. Structural interpretation of the energetic performances of a pure silica LTA-type zeolite. *Phys. Chem. Chem. Phys.* **2020**, *22*, 5178−5187.
(31) Ryzhikov, A.; Ronchi, L.; Nouali, H.; Daou, T. J.; Paillaud, J.-L.; Patarin, J. High-pressure intrusion−extrusion of water and electrolyte solutions in pure-silica LTA zeolite. *J. Phys. Chem. C* **2015**, *119*, 28319−28325.
(32) Huve, J.; Daou, T. J.; Nouali, H.; Patarin, J.; Ryzhikov, A. The effect of nanostructures on high pressure intrusion−extrusion of water and electrolyte solutions in hierarchical nanoboxes of silicalite-1. *New J. Chem.* **2020**, *44*, 273−281.
(33) Ronchi, L.; Ryzhikov, A.; Nouali, H.; Daou, T.; Patarin, J. Influence of LiCl aqueous solution concentration on the energetic performances of pure silica chabazite. *New J. Chem.* **2017**, *41*, 2586−2592.
(34) Isaac, C.; Confalonieri, G.; Nouali, H.; Paillaud, J.-L.; Arletti, R.; Daou, T. J.; Ryzhikov, A. Unusual high-pressure intrusion-extrusion behavior of electrolyte solutions in Mu-26, a pure silica zeolite of topology STF. *Microporous Mesoporous Mater.* **2020**, *298*, 110047.
(35) Ronchi, L.; Nouali, H.; Daou, T. J.; Patarin, J.; Ryzhikov, A. Heterogeneous lyophobic systems based on pure silica ITH-type zeolites: High pressure intrusion of water and electrolyte solutions. *New J. Chem.* **2017**, *41*, 15087−15093.
(36) Confalonieri, G.; Daou, T. J.; Nouali, H.; Arletti, R.; Ryzhikov, A. Energetic performance of pure silica zeolites under high-pressure intrusion of LiCl aqueous solutions: an overview. *Molecules* **2020**, *25*, 2145.
(37) Ronchi, L.; Ryzhikov, A.; Nouali, H.; Daou, T. J.; Albrecht, S.; Patarin, J. Investigation of the energetic performance of pure silica BEC-type zeolite under high pressure water and 20 M LiCl intrusion-extrusion experiments. *Microporous Mesoporous Mater.* **2017**, *254*, 153−159.
(38) de Izarra, A.; Coudert, F.-X.; Fuchs, A. H.; Boutin, A. Predictive Thermodynamic Model for Intrusion of Electrolyte Aqueous Solutions in Nanoporous Materials. *ChemRxiv* **2023**.
(39) Pitzer, K. S.; Press, C. *Activity coefficients in electrolyte solutions*; CRC Press: Boca Raton, FL, 1991; Vol. *2*.
(40) Humphreys, M. P.; Schiller, A. J. *Pytzer: the Pitzer model for chemical activities and equilibria in aqueous solutions in Python (beta)*, 2021.
(41) Barrer, R. *Hydrothermal synthesis of zeolites*; Academic Press, 1982.
(42) Guth, J.; Kessler, H.; Caullet, P.; Hazm, J.; Merrouche, A.; Patarin, J. F. A multifunctional tool for microporous solids. (a) Mineralizing, structure directing and templating effects in the synthesis. *Proceedings from the Ninth International Zeolite Conference*, 1993; pp 215−222.
(43) Corma, A.; Rey, F.; Rius, J.; Sabater, M. J.; Valencia, S. Supramolecular self-assembled molecules as organic directing agent for synthesis of zeolites. *Nature* **2004**, *431*, 287−290.
(44) Murakami, Y.; Iijima, A.; Ward, J. W. *New Developments in Zeolite Science and Technology*; Elsevier, 1986.
(45) Cailliez, F.; Stirnemann, G.; Boutin, A.; Demachy, I.; Fuchs, A. H. Does water condense in hydrophobic cavities? A molecular simulation study of hydration in heterogeneous nanopores. *J. Phys. Chem. C* **2008**, *112*, 10435−10445.
(46) Olson, D.; Kokotailo, G.; Lawton, S.; Meier, W. Crystal structure and structure-related properties of ZSM-5. *J. Phys. Chem.* **1981**, *85*, 2238−2243.
(47) Calligaris, M.; Nardin, G.; Randaccio, L. Cation site location in hydrated chabazites. Crystal structure of potassium-and silver-exchanged chabazites. *Zeolites* **1983**, *3*, 205−208.
(48) Fuchs, A. H.; Cheetham, A. K. Adsorption of Guest Molecules in Zeolitic Materials: Computational Aspects. *J. Phys. Chem. B* **2001**, *105*, 7375−7383.
(49) Chezeau, J.; Delmotte, L.; Guth, J.; Gabelica, Z. Influence of synthesis conditions and postsynthesis treatments on the nature and quantity of structural defects in highly siliceous MFI zeolites: A high-resolution solid-state ^{29}Si NMR study. *Zeolites* **1991**, *11*, 598−606.
(50) Barrer, R.; Makki, M. Molecular sieve sorbents from clinoptilolite. *Can. J. Chem.* **1964**, *42*, 1481−1487.
(51) Qin, Z.; Zeng, S.; Melinte, G.; Bučko, T.; Badawi, M.; Shen, Y.; Gilson, J.; Ersen, O.; Wei, Y.; Liu, Z.; et al. Understanding the Fundamentals of Microporosity Upgrading in Zeolites: Increasing Diffusion and Catalytic Performances. *Adv. Sci.* **2021**, *8*, 697.
(52) Dubbeldam, D.; Calero, S.; Ellis, D. E.; Snurr, R. Q. RASPA: molecular simulation software for adsorption and diffusion in flexible nanoporous materials. *Mol. Simul.* **2016**, *42*, 81−101.
(53) Steinhauser, M. O. A molecular dynamics study on universal properties of polymer chains in different solvent qualities. Part I. A review of linear chain properties. *J. Chem. Phys.* **2005**, *122*, 094901.
(54) Sokol, A. A.; Catlow, C. R. A.; Garcés, J. M.; Kuperman, A. Local states in microporous silica and aluminum silicate materials. 1. Modeling structure, formation, and transformation of common hydrogen containing defects. *J. Phys. Chem. B* **2002**, *106*, 6163−6177.
(55) Purton, J.; Jones, R.; Heggie, M.; Öberg, S.; Catlow, C. LDF pseudopotential calculations of the α-quartz structure and hydrogarnet defect. *Phys. Chem. Miner.* **1992**, *18*, 389−392.
(56) Desbiens, N.; Boutin, A.; Demachy, I. Water condensation in hydrophobic silicalite-1 zeolite: a molecular simulation study. *J. Phys. Chem. B* **2005**, *109*, 24071−24076.
(57) Jorgensen, W. L.; Chandrasekhar, J.; Madura, J. D.; Impey, R. W.; Klein, M. L. Comparison of simple potential functions for simulating liquid water. *J. Chem. Phys.* **1983**, *79*, 926−935.
(58) Chowdhuri, S.; Chandra, A. Hydration structure and diffusion of ions in supercooled water: Ion size effects. *J. Chem. Phys.* **2003**, *118*, 9719−9725.
(59) Mamatkulov, S.; Fyta, M.; Netz, R. R. Force fields for divalent cations based on single-ion and ion-pair properties. *J. Chem. Phys.* **2013**, *138*, 024505.
(60) Izarra, A. d.; Coudert, F.-X.; Fuchs, A. H.; Boutin, A. Alchemical Osmostat for Monte Carlo Simulation: Sampling Aqueous Electrolyte Solution in Open Systems. *J. Phys. Chem. B* **2023**, *127*, 766−776.
(61) Nilmeier, J. P.; Crooks, G. E.; Minh, D. D.; Chodera, J. D. Nonequilibrium candidate Monte Carlo is an efficient tool for equilibrium simulation. *Proc. Natl. Acad. Sci. U.S.A.* **2011**, *108*, E1009−E1018.
(62) Ross, G. A.; Rustenburg, A. S.; Grinaway, P. B.; Fass, J.; Chodera, J. D. Biomolecular simulations under realistic macroscopic salt conditions. *J. Phys. Chem. B* **2018**, *122*, 5466−5486.
(63) Rouquerol, J.; Rouquerol, F.; Llewellyn, P.; Maurin, G.; Sing, K. *Adsorption by powders and porous solids: principles, methodology and applications*; Academic Press, 2013.
(64) Loche, P.; Steinbrunner, P.; Friedowitz, S.; Netz, R. R.; Bonthuis, D. J. Transferable ion force fields in water from a simultaneous optimization of ion solvation and ion−ion interaction. *J. Phys. Chem. B* **2021**, *125*, 8581−8587.

https://doi.org/10.1021/acs.langmuir.3c03306
Langmuir 2023, 39, 19056−19063